2010 IEEE International Conference on Robotics and Automation
Anchorage Convention District
May 3-8, 2010, Anchorage, Alaska, USA

A Study of Bouncing Rod Dynamics Aiming at Passive Running

Hiroki Miyamoto, Akihito Sano, Yoshito Ikemata, Shintaro Maruyama, and Hideo Fujimoto

Abstract— **Passive running robot can run down shallow slope with no energy source without gravity. The robot can generate a stable limit cycle. Dynamics of passive running is very interesting target and important for developing the robot and understanding the human locomotion. By the way, running high jumper can jump very high. The point of jumping is to transfer horizontal velocity into lifting momentum through the hinged-movement. In this paper, we demonstrate the experimental passive running based on the hinged-movement. Moreover, we derive the fixed point of the passive running, and analyze its stability.**

I. INTRODUCTION

Biped locomotion is a very attractive mode for robot movement. Cutting-edge running robots can run fast and stably. Main concerns of these robots are selection of actuator, mechanism design, and system control. Jumping is a very difficult problem. While, passive running robot can run by interaction between machine dynamics and environment only. 1-legged [1][2][3], 2-legged [4][5], and 4-legged [6] passive running exist. Each leg has a translational spring, which allows for compression during stance, and the subsequent rebound into the flight phase.

Passive running can be regarded as a physical phenomenon generated by the hybrid system, which consist of the continuous dynamics of leg-swing motion and the discrete event of collision. Passive running robot can exhibit a stable limit cycle like passive walking [7][8][9][10]. When the state keeps on the stable limit cycle, the running system is stable. Passive running may give us an insight into understanding the human locomotion and developing the robots.

By the way, a bar can jump rotating when it is properly thrown out to the flat ground. The point of jumping is to transfer horizontal velocity into lifting momentum. This phenomenon is called "hinged-movement". High jumper can jump very high by the principle of hinged-movement. This paper focuses on the running robot using the hinged-movement and not the robot using spring [11][12][13].

In this paper, we propose a passive running based on the hinged-movement. First, the hinged-movement is conformed by the experiment, and is modeled based on the experimental result. Secondly, passive running based on the hinged-movement is demonstrated by the experiment. Thirdly, fixed point is derived analytically. Finally, stability of the fixed point is demonstrated by the simulation.

H. Miyamoto, A. Sano, Y. Ikemata, and H. Fujimoto are with Nagoya Institute of Technology, Gokiso-cho, Showa-ku, Nagoya, Aichi, 466-8555, JAPAN ikemata@vier.mech.nitech.ac.jp

(a) Photo of glass fiber bar

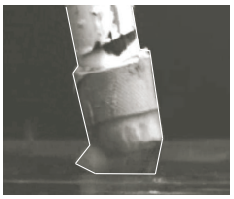

(b) Shear deformation of urethane cap

Fig. 1. Hinged-movement bar

II. HINGED-MOVEMENT

A. Basic experiment

Figure 1 (a) shows a bar, which was used in hinged-movement experiments. The bar was made by the glass fiber for pole vault. Diameter and length of the bar are 0.026 and 1.93[m] respectively. Mass is 0.78[kg]. Inertia moment about center of gravity is 0.2424[kgm^2]. Urethane caps were attached in both ends of the bar. We did a basic experiment for hinged-movement of the bar. Figure 1 (b) shows a collision between the bar and the ground. The urethane cap makes shear. Horizontal direction speed at the collision is 4[m/s]. The contact time is only 8[ms].

Position of center of the bar x, y and posture θ are shown in Fig. 2 (a), (b), and (c) respectively. Please see Fig. 3 for the details of the coordinates. The bar had a collision with ground at 0.063[s]. Posture of the bar is backward inclining. After the collision, the bar jumped rotating.

B. Modeling

Figure 3 shows the model of hinged-movement. M is mass. I is moment of inertia about center of gravity. l is distance between the center of gravity and the end of bar. Horizontal and vertical positions of the center of gravity are x and y respectively. Equations of motion of flight phase can be obtained as follows:

$$\begin{cases} M\ddot{x} = 0 \\ M\ddot{y} = -Mg \\ I\ddot{\theta} = 0 \end{cases} \tag{1}$$

Collision is very short time (8[ms]). Therefore, we assumed that the bar bounds in axial direction instantaneously.

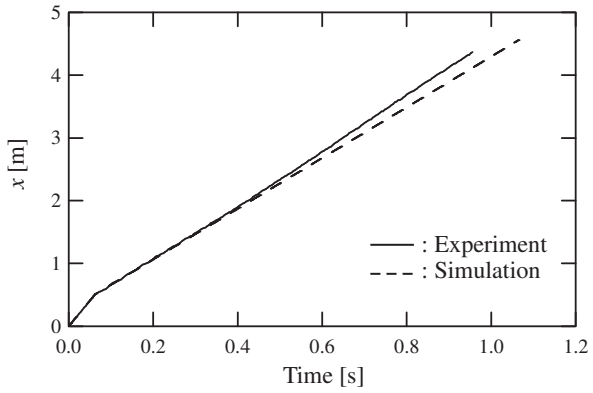

(a) x

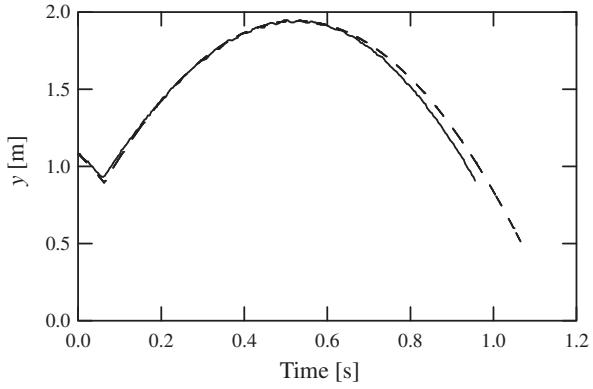

(b) y

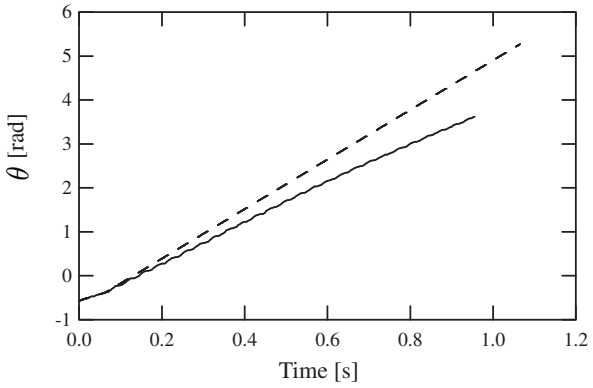

(c) θ

Fig. 2. Position and posture of bar

Relational expression of axial velocity just before and after collision can be obtained as

$$\dot{L}^{+} = -e\dot{L}^{-} \tag{2}$$

where

$$\dot{L}^{-} = \dot{x}^{-}\sin(\theta^{+} + \gamma) + \dot{y}^{-}\cos(\theta^{+} + \gamma)$$

L is length of the bar. $\theta^{+} = \theta^{-}$ holds. The "+" superscript means "just after collision," and the "−" superscript means "just before collision". e is coefficient of restitution at collision ($0 < e < 1$).

In addition, angular momentum is conserved through collision. From this conservation of angular momentum,

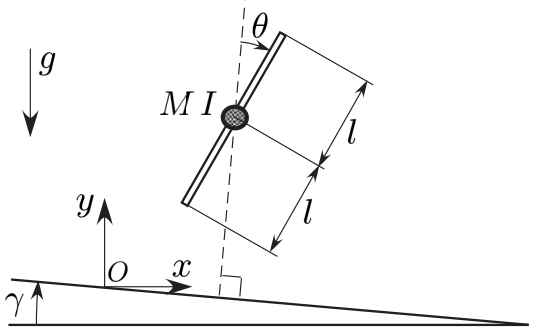

Fig. 3. Model of hinged-movement

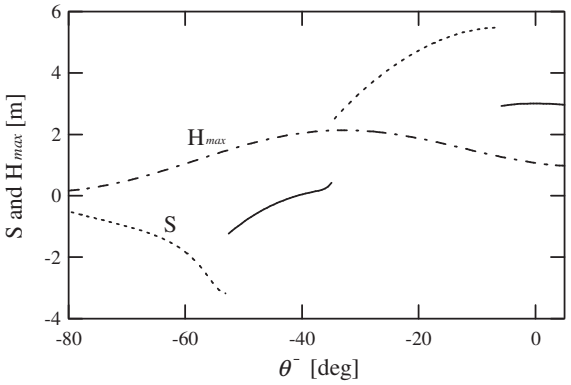

Fig. 4. Step length and maximum height

relational expression can be obtained as

$$\dot{\theta}^{+} = \frac{Ml\{\dot{x}^{-}\cos(\theta^{+} + \gamma) - \dot{y}^{-}\sin(\theta^{+} + \gamma)\} + I\dot{\theta}^{-}}{Ml^2 + I} \tag{3}$$

C. Simulation

Simulation results are shown in Fig. 2. Model parameters were decided by the experimental bar. Coefficient of restitution e is decided by a simple collision experiment. e was set to 0.44. As seen from Fig. 2, there are a few errors between the simulation results and experimental results. Features of the simulation results correspond to the those of experiment results. Therefore, it seems that the model is appropriate.

We run simulations for various posture angles at collision as shown in Fig. 4. The translational and angular velocities just before collision are fixed. The horizontal axis denotes the posture angle just before collision θ^{-}. The vertical axis denotes the jumping distance S and maximum height of the center of mass H_{max}. The continuous line represents the jump distance S in case that opposite edge of bar collides on the ground. The dashed line represents the jump distance S in case that same edge of bar collides on the ground. The dash-dot line represents the maximum height of the center of mass H_{max}.

As seen from Fig. 4, the maximum height H_{max} changes for the posture angle at collision. H_{max} has maximum at θ^{-} = –35[deg]. In case of the high jump, this posture angle is important. While, in case of the jump distance, it is desired that posture angle θ^{-} is near zero.

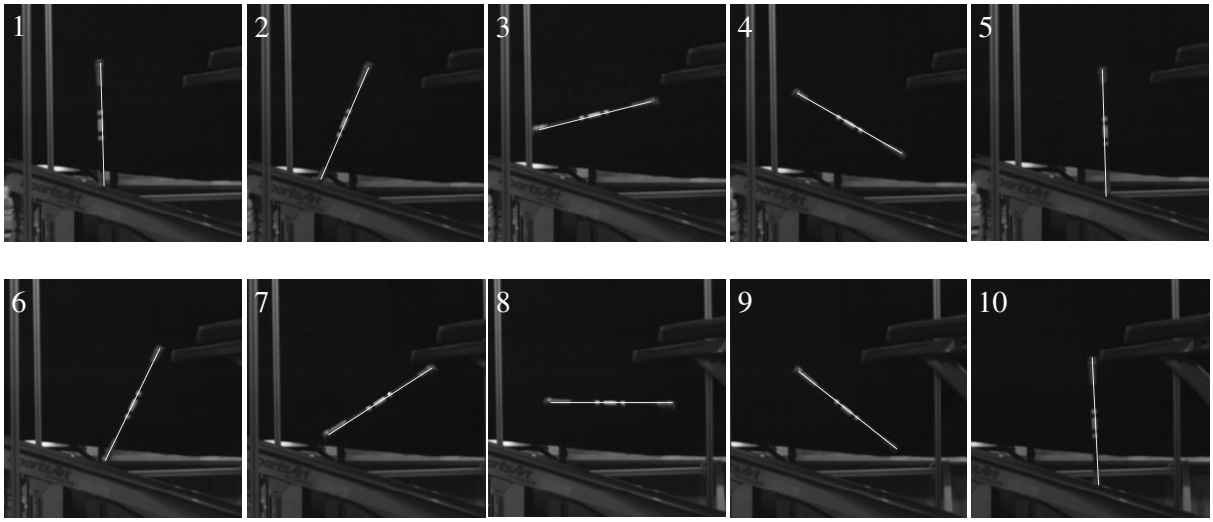

Fig. 5. A photographic playback of passive running based on hinged-movement

III. Passive running based on hinged-movement

A. Experimental condition

On the level ground, the hinged-movement cannot be continued because there is no energy supply. Therefore, we did an experiment of hinged-movement on slope like passive walking. We used a treadmill because experiment space is limited. Length and width of the treadmill are 1.3 and 0.5[m] respectively. Belt speed of the treadmill is constant. In addition, the bar was shortened.

In order to reduce the rotation speed of bar, a weight is put in the bar. Length of bar is 57[cm]. Mass is 460[g]. Inertia moment is 0.0125[kgm^2]. When the bar was dropped on the ground, rebound of the bar was very small.

B. Experimental results

Experiments by trial and error showed that the best slope angle is 18.5[deg]. Belt speed of the treadmill is about 14.5[km/h]. Though the success rate was not high, we succeeded in 9 steps of passive running based on the hinged-movement. Figure 5 shows a photographic playback of passive running based on the hinged-movement. The movement is beautiful like a floor exercise of the gymnast.

Figure 6 shows the experimental result. The horizontal axis denotes the time. The vertical axis denotes the posture angle of bar θ. The posture angle at collision is almost vertical. This result means that best posture angle at collision is vertical.

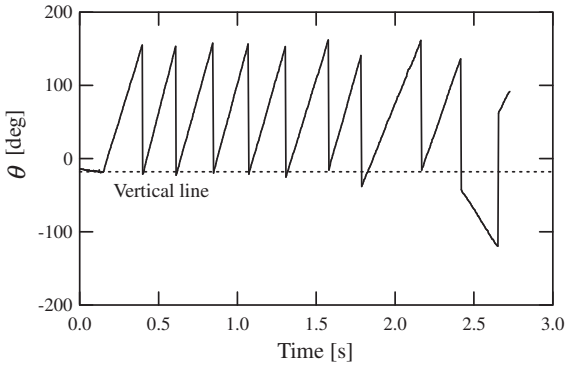

Fig. 6. Experimental result of passive running

IV. Fixed point

A. Collision time

Running system generates a cyclic trajectory. When the trajectory is limit cycle, the state just after collision is fixed as one point. This point is called "fixed point". In this paper, we analyze the fixed point of one cycle. The state just after collision of k step is represent by θ_k^+, $\dot{\theta}_k^+$ and $\dot{L_k}^+$. In the fixed point, $\theta_{k+1}^+ = \theta_k^+$, $\dot{\theta}_{k+1}^+ = \dot{\theta}_k^+$ and $\dot{L}_{k+1}^+ = \dot{L}_k^+$ hold.

When the posture angle at collision of k steps is equal to the one of $k+1$ steps, we can obtain the equation as follows:

$$\theta_{k+1}^- = \theta_k^+ + \pi \tag{4}$$

Initial state is set to the state just after collision of k steps. The position of center of gravity at time t can be obtained as

$$x_t = \dot{x}_k^+ t \qquad y_t = \dot{y}_k^+ t - \frac{1}{2} g t^2 \tag{5}$$

From Eq. (5), the trajectory of center of gravity can be derived as follows:

$$y_t = \frac{\dot{y}_k^+}{\dot{x}_k^+} x_t - \frac{1}{2} \frac{g}{\dot{x}_k^{+2}} x_t^2 \tag{6}$$

In the fixed point, the posture just after collision of $k+1$ steps is equal to the one of k. From this geometric condition, the position of fixed point must be located on the line trajectory as follows:

$$y_t = -x_t \tan\gamma \tag{7}$$

From Eqs. (6) and (7), position x_f of the fixed point can be derived as

$$x_f = \frac{2\dot{x}_k^+(\dot{y}_k^+ + \dot{x}_k^+ \tan\gamma)}{g} \tag{8}$$

From Eqs. (5) and (8), the flight time t_f of the fixed point can be derived as follows:

$$t_f = \frac{2(\dot{y}_k^+ + \dot{x}_k^+ \tan\gamma)}{g} \tag{9}$$

In addition, the translation velocity and the angular velocity just before collision of $k+1$ steps can be derived as follows.

$$\dot{x}_{k+1}^- = \dot{x}_k^+ \tag{10}$$

$$\begin{aligned}\dot{y}_{k+1}^- &= \dot{y}_k^+ - gt_f \\ &= -\dot{y}_k^+ - 2\dot{x}_k^+ \tan\gamma \end{aligned} \tag{11}$$

$$\dot{\theta}_{k+1}^- = \dot{\theta}_k^+ \tag{12}$$

B. Necessary condition of fixed point

From Eqs. (10) and (12), fixed point can be generated when the equation (13) meets.

$$\dot{x}_{k+1}^+ = \dot{x}_{k+1}^- \qquad \dot{\theta}_{k+1}^+ = \dot{\theta}_{k+1}^- \tag{13}$$

Equation (13) means that horizontal speed $\dot{x}$ and angular velocity $\dot{\theta}$ don't change at collision. In order to meet Eq. (13), the following relational equations must hold. This relational equations can be obtained from Eq. (3).

$$\theta_k^+ = -\gamma \qquad l\dot{\theta}_k^+ = \dot{x}_k^+ \tag{14}$$

Equation (13) means that the posture at collision is vertical, and the horizontal velocity of edge of bar is zero. Therefore, the bar collides with ground in the vertical direction. From this condition, the equation can be obtained as follows:

$$\dot{y}_{k+1}^- = -\frac{\dot{y}_k^+}{e} \tag{15}$$

$$\dot{L}_k^+ = \dot{y}_k^+ \tag{16}$$

The condition equation of fixed point ($\dot{y}_{k+1}^- = \dot{y}_k^-$) and Eq. (15) are substituted for Eq. (11). So, we can obtain the equation as

$$\dot{y}_k^+ = \frac{2e\tan\gamma}{1-e}\dot{x}_k^+ \tag{17}$$

In addition, the bar must rotate by 180[deg] at the flight phase in the fixed point. From this condition, we can obtain the equation as

$$\begin{aligned}\pi &= \dot{\theta}_k^+ t \\ &= \frac{2\dot{\theta}_k^+(\dot{y}_k^+ + \dot{x}_k^+ \tan\gamma)}{g} \end{aligned} \tag{18}$$

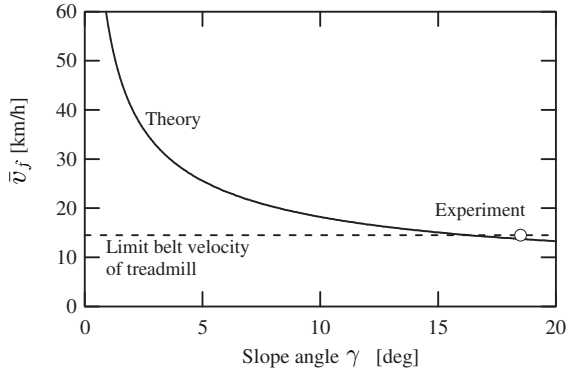

Fig. 7. Slope angle and average velocity

C. Fixed point and average velocity

From Eqs. (14), (16), (17), and (18), fixed point of one cycle can be derived as follows:

$$\theta_f^+ = -\gamma \tag{19}$$

$$\dot{\theta}_f^+ = \sqrt{\frac{(1-e)\pi g}{2(1+e)\,l\tan\gamma}} \tag{20}$$

$$\dot{L}_f^+ = \sqrt{\frac{2e^2\pi l g\tan\gamma}{(1+e)(1-e)}} \tag{21}$$

One fixed point exists when coefficient of restitution at the collision is $0 < e < 1$. In the fixed point, the posture angle at collision is vertical. This feature corresponds with the experimental feature that the posture angle at collision is almost vertical.

From moving distance and time, average velocity of the fixed point can be derived as follows:

$$\begin{aligned}\bar{v}_f &= \frac{\dot{x}_f^+ t_f}{t_f\cos\gamma} \\ &= \sqrt{\frac{(1-e)\pi l g}{(1+e)\sin 2\gamma}} \end{aligned} \tag{22}$$

Figure 7 shows the average velocity $\bar{v}_f$ with slope angles γ. Model parameters were decided by the experimental bar. Coefficient of restitution e was assumed to be 0.001. Small circle in Fig. 7 represents the experimental result. Dashed line represents the limit velocity of the treadmill.

When slope angle γ increases, the average velocity $\bar{v}_f$ becomes slow. In case that slope angle γ is small, it is very difficult to generate the passive running because the moving velocity of the fixed point exceeds the limit velocity of the treadmill. In the experiment, the slope angle γ must be set to more than 16 [deg]. Slope angle γ of the experiment is 18.5[deg]. In addition, the velocity of experiment corresponds with the theoretical value.

V. Stability of fixed point

A. Unstable fixed point

State quantities of the state just after collision are expressed as $\boldsymbol{x}_k^+ = [\theta_k^+,\ \dot{\theta}_k^+,\ \dot{L}_k^+]^T$. Successive states is related

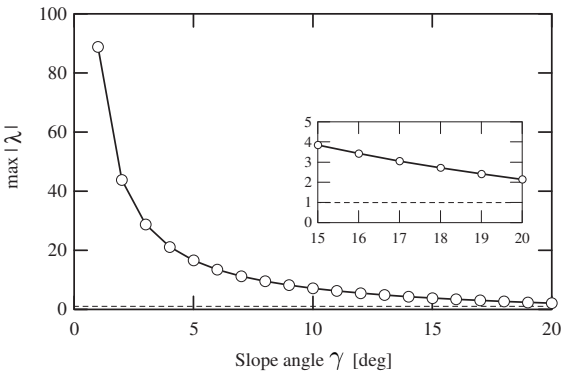

Fig. 8. Slope angle and max $|\lambda|$

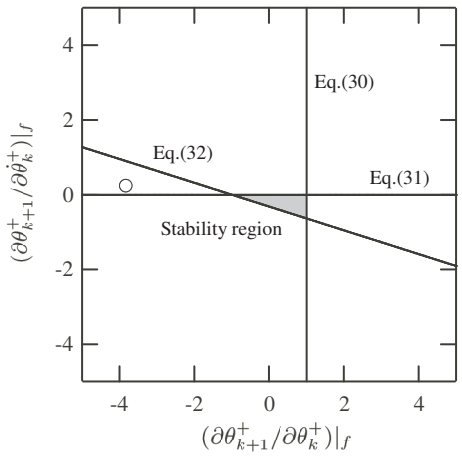

Fig. 9. Stability region

as

$$\boldsymbol{x}^+_{k+1} = f(\boldsymbol{x}^+_k) \tag{23}$$

Fixed point is expressed as $\boldsymbol{x}^+_f$. Fixed point is related as $\boldsymbol{x}^+_f = f(\boldsymbol{x}^+_f)$. For a small perturbation $\Delta\boldsymbol{x}^+_k$ around fixed point, f is expressed in term of Taylor series expansion as

$$\boldsymbol{x}^+_{k+1} = f(\boldsymbol{x}^+_f) + \left.\frac{\partial f}{\partial \boldsymbol{x}^+}\right|_{\boldsymbol{x}^+=\boldsymbol{x}^+_f} \Delta\boldsymbol{x}^+_k \tag{24}$$

From Eqs.(23) and (24), linear discrete-time state equation is derived as

$$\Delta\boldsymbol{x}^+_{k+1} = \left.\frac{\partial f}{\partial \boldsymbol{x}^+}\right|_{\boldsymbol{x}^+=\boldsymbol{x}^+_f} \Delta\boldsymbol{x}^+_k \equiv \boldsymbol{J}_f \Delta\boldsymbol{x}^+_k \tag{25}$$

where

$$\boldsymbol{J}_f = \begin{bmatrix} \left.\frac{\partial\theta^+_{k+1}}{\partial\theta^+_k}\right|_f & \left.\frac{\partial\theta^+_{k+1}}{\partial\dot\theta^+_k}\right|_f & \left.\frac{\partial\theta^+_{k+1}}{\partial\dot L^+_k}\right|_f \\ \left.\frac{\partial\dot\theta^+_{k+1}}{\partial\theta^+_k}\right|_f & \left.\frac{\partial\dot\theta^+_{k+1}}{\partial\dot\theta^+_k}\right|_f & \left.\frac{\partial\dot\theta^+_{k+1}}{\partial\dot L^+_k}\right|_f \\ \left.\frac{\partial\dot L^+_{k+1}}{\partial\theta^+_k}\right|_f & \left.\frac{\partial\dot L^+_{k+1}}{\partial\dot\theta^+_k}\right|_f & \left.\frac{\partial\dot L^+_{k+1}}{\partial\dot L^+_k}\right|_f \end{bmatrix} \tag{26}$$

If all absolute eigenvalues of Jacobian matrix $\boldsymbol{J}_f$ are less than one, fixed point is local asymptotically stable.

Figure 8 shows the maximum of absolute eigenvalues of Jacobian matrix with slope angles γ. Jacobian matrix was obtained from the simulation. The fixed point is unstable because $\max|\lambda|$ is larger than one. When slope angle γ increases, instability of fixed point decreases. In the experiment, success rate of passive running increases when slope angle γ increases. This experimental feature corresponds with the theoretical analysis.

B. Simplification of Jacobian matrix

One of the eigenvalues of Jacobian matrix is almost zero because the axial velocity just after collision $\dot L^+$ is almost zero. Therefore, the state quantities of the state just after collision can be expressed as $\boldsymbol{x}^+_k = [\theta^+_k,\ \dot\theta^+_k]^T$. $(\partial\dot\theta^+_{k+1}/\partial\theta^+_k)|_f$ and $(\partial\dot\theta^+_{k+1}/\partial\dot\theta_k)|_f$ in $\boldsymbol{J}_f$ can be obtained as follows:

$$\left.\frac{\partial\dot\theta^+_{k+1}}{\partial\theta^+_k}\right|_f = a_f \left.\frac{\partial\theta^+_{k+1}}{\partial\theta^+_k}\right|_f \tag{27}$$

$$\left.\frac{\partial\dot\theta^+_{k+1}}{\partial\dot\theta^+_k}\right|_f = a_f \left.\frac{\partial\theta^+_{k+1}}{\partial\dot\theta^+_k}\right|_f + 1 \tag{28}$$

where

$$a_f = \frac{Ml\pi g}{Ml^2 + I}\sqrt{\frac{2(1+e)l\tan\gamma}{(1-e)\pi g}}$$

See the appendix for the detail of derivation of Eqs (27) and (28).

Jacobian matrix $\boldsymbol{J}_f$ of Eq. (26) can be written as follows:

$$\boldsymbol{J}_f = \begin{bmatrix} \left.\frac{\partial\theta^+_{k+1}}{\partial\theta^+_k}\right|_f & \left.\frac{\partial\theta^+_{k+1}}{\partial\dot\theta^+_k}\right|_f \\ a_f \left.\frac{\partial\theta^+_{k+1}}{\partial\theta^+_k}\right|_f & a_f \left.\frac{\partial\theta^+_{k+1}}{\partial\dot\theta^+_k}\right|_f + 1 \end{bmatrix} \tag{29}$$

C. Stability region of fixed point

From Eq. (29), equations of stability condition of the fixed point can be derived as follows:

$$\left.\frac{\partial\theta^+_{k+1}}{\partial\theta^+_k}\right|_f < 1 \tag{30}$$

$$a_f \left.\frac{\partial\theta^+_{k+1}}{\partial\dot\theta^+_k}\right|_f < 0 \tag{31}$$

$$-a_f \left.\frac{\partial\theta^+_{k+1}}{\partial\dot\theta^+_k}\right|_f - 2\left.\frac{\partial\theta^+_{k+1}}{\partial\theta^+_k}\right|_f < 2 \tag{32}$$

When $(\partial\theta^+_{k+1}/\partial\theta^+_k)|_f$ and $(\partial\dot\theta^+_{k+1}/\partial\dot\theta^+_k)|_f$ meet Eqs. (30), (31), and (32), the fixed point is local-asymptotically stable.

Figure 9 shows the stability region as the shaded area. Horizontal and vertical axes denote $(\partial\theta^+_{k+1}/\partial\theta^+_k)|_f$ and $(\partial\dot\theta^+_{k+1}/\partial\dot\theta^+_k)|_f$ respectively. $(\partial\theta^+_{k+1}/\partial\theta^+_k)|_f$ and $(\partial\dot\theta^+_{k+1}/\partial\dot\theta^+_k)|_f$ of fixed poin are obtained by numerical analysis. The location is overlaid as the small circle in Fig. 9. The fixed point

is unstable because the small circle is not located in the stability region. However, the stability region exists. In order to stabilize the fixed point, $(\partial\theta^+_{k+1}/\partial\theta^+_k)|_f$ and $(\partial\theta^+_{k+1}/\partial\dot{\theta}^+_k)|_f$ must be put in the stability region.

VI. Conclusions

In this paper, we did experiments and analyzed a passive running based on the hinged-movement. The results of this study are summarized as follows:

(1) We realized passive running based on the hinged-movement. The movement is beautiful like a floor exercise of the gymnast. Average speed of the passive running is very high (14.5[km/h]).

(2) Fixed point of the passive running was derived analytically. In the fixed point, the posture angle at collision is vertical. When slope angle increases, the moving speed becomes slow.

(3) Stability of the fixed point was demonstrated from the eigenvalues of Jacobian matrix. The fixed point is unstable. When slope angle increases, instability of fixed point decreases.

(4) By simplifying Jacobian matrix, equations of stability condition of the fixed point were derived analytically. Though the stability region exists, the fixed point is not located in the stability region. Therefore, the fixed point becomes unstable.

Video footage of the experiment can be seen on WWW (http://drei.mech.nitech.ac.jp/˜fujimoto/sano/walk_eng.html). In the future, we will derive the stabilization method of the fixed point. We will realize a stable passive running based on thehinged-movement.

VII. Acknowledgments

This work was partially supported by a Grant-in-Aid for Scientific Research (A) No. 21246042, and a Grant-in-Aid for Young Scientists (B) No. 20760167, provided by the Japan Society for the Promotion of Science.

References

[1] S. Hyon and T. Emura, "Quasi-Periodic Gait of Passive One legged Hopper," *Proceedings of 2002 IEEE/RSJ International Conference on Intelligent Robots and Systems*, pp.2625–2630, 2002.

[2] S. Satoshi et al., "Gait Generation for Passive Running via Iterative Learning Control," *Proceedings of 2006 IEEE/RSJ International Conference on Intelligent Robots and Systems*, pp.5907–5912, 2006.

[3] M. Ahmadi and M. Buehler, "Controlled Passive Dynamic Running Experiments With the ARL-Monopod II," *IEEE Transactions on Robotics*, vol.22, no.5, pp.974–986, 2006.

[4] T. McGeer, "Passive Bipedal Running," *Proc. of the Royal Society of London. Series B, Biological Sciences*, vol.240, no.1297, pp.107–134, 1990.

[5] D. Owaki et al., "On the Embodiment That Enables Passive Bipedal Running," *Proceedings of the 2008 IEEE International Conference on Robotics and Automation*, pp.341–346, 2008.

[6] Z. G. Zhang, "Autonomously Generating Efficient Running of a Quadruped Robot Using Delayed Feedback Control," *Advanced Robotics*, vol.20, no.6, pp.607–629, 2006.

[7] T. McGeer, "Passive Dynamic Walking," *The Int. J. of Robotics Research*, vol.9, no.2, pp.62–68, 1990.

[8] A. Goswami, B. Thuilot, and B. Espiau, "A Study of the Passive Gait of a Compass-Like Biped Robot : Symmetry and Chaos," *The Int. J. of Robotics Research*, pp.1282–1301, 1998.

[9] M. Garcia, A. Chatterjee, A. Ruina, and M. Coleman, "The Simplest Walking Model : Stability, Complexity, and Scaling," *ASME J. of Biomechanical Engineering*, pp.281–288, 1998.

[10] Y. Ikemata, A. Sano, K. Yasuhara, and H. Fujimoto, "Dynamic Effects of Arc Feet on the Leg Motion of Passive Walker," *Proc. of the 2009 IEEE Int. Conf. on Robotics and Automation*, pp.2755–2760, 2009.

[11] M. H. Raibert, "Legged Robots That Balance," The MIT Press, 1986.

[12] A. Setfarth et al., "Swing-leg Retraction: A Simple Control Model for Stable Running," *J. of Experimental Biology*, vol.206, pp.2547–2555, 2003.

[13] H. Miyamoto, Y. Ikemata, A. Sano, and H. Fujimoto, "Passive Running of Rimless Wheel with Springs," *Proceedings of the 2009 Int. Conf. on Climbing and Walking Robots and the Supporting Technologies for Mobile Machines*, pp.269–276, 2009.

Appendix

Time t_{k+1} from k steps to $k+1$ steps can be written as follows:

$$\begin{aligned} t_{k+1} &= \frac{\theta^-_{k+1} - \theta^+_k}{\dot{\theta}^+_k} \\ &= \frac{\theta^+_{k+1} - \theta^+_k + \pi}{\dot{\theta}^+_k} \end{aligned} \tag{33}$$

Horizontal and vertical velocities just after collision of step k can be obtained as

$$\dot{x}^+_k = l\dot{\theta}^+_k \cos\left(\theta^+_k + \gamma\right) \tag{34}$$

$$\dot{y}^+_k = -l\dot{\theta}^+_k \sin\left(\theta^+_k + \gamma\right) \tag{35}$$

Translational velocity just before collision of step $k+1$ can be derived as follows:

$$\dot{x}^-_{k+1} = \dot{x}^+_k = l\dot{\theta}^+_k \cos\left(\theta^+_k + \gamma\right) \tag{36}$$

$$\begin{aligned} \dot{y}^-_{k+1} &= \dot{y}^+_k - gt_{k+1} \\ &= -l\dot{\theta}^+_k \sin\left(\theta^+_k + \gamma\right) - g\frac{\theta^+_{k+1} - \theta^+_k + \pi}{\dot{\theta}^+_k} \end{aligned} \tag{37}$$

From Eqs. (3), (36) and (37), discrete-time state equation of $\dot{\theta}^+_k$ can be derived as follows:

$$\begin{aligned} \dot{\theta}^+_{k+1} = &\frac{Ml^2\dot{\theta}^+_k \cos\left(\theta^+_k + \gamma\right)\cos\left(\theta^+_{k+1} + \gamma\right)}{Ml^2 + I} \\ &+ \frac{Ml^2\dot{\theta}^+_k \sin\left(\theta^+_k + \gamma\right)\sin\left(\theta^+_{k+1} + \gamma\right)}{Ml^2 + I} \\ &+ \frac{Mlg\left(\theta^+_{k+1} - \theta^+_k + \pi\right)\sin\left(\theta^+_{k+1} + \gamma\right)}{\dot{\theta}^+_k\left(Ml^2 + I\right)} \\ &+ \frac{I\dot{\theta}^+_k}{Ml^2 + I} \end{aligned} \tag{38}$$

By linearizing and differentiating Eq. (38), Eqs. (27) and (28) can be derived.